Passive and active microrheology for cross-linked F-actin networks *in vitro*

Hyungsuk Lee[*], Jorge M. Ferrer[†], Fumihiko Nakamura[‡], Matthew J. Lang[*†], and Roger D. Kamm[*†]

[*]Departments of Mechanical Engineering, Massachusetts Institute of Technology, Cambridge, MA 02139, USA
[†]Departments of Biological Engineering, Massachusetts Institute of Technology, Cambridge, MA 02139, USA
[‡]Translational Medicine Division, Brigham and Women's Hospital, Department of Medicine, Harvard Medical School, Boston, MA 02115, USA

Corresponding Author:
Roger D. Kamm, Ph.D.
Massachusetts Institute of Technology, Department of Mechanical and Biological Engineering
77 Massachusetts Avenue, Room NE47-321, Cambridge MA 02139, USA
Email: rdkamm@mit.edu
Telephone: 1-617-253-5330 / Fax: 1-617-258-8559

Abstract

Actin filament (F-actin) is one of the dominant structural constituents in the cytoskeleton. Orchestrated by various actin binding proteins (ABPs), F-actin is assembled into higher-order structures such as bundles and networks that provide mechanical support for the cell and play important roles in numerous cellular processes. Although mechanical properties of F-actin networks have been extensively studied, the underlying mechanisms for network elasticity is not fully understood, in part because different measurements probe different length and force scales. Here, we developed both *passive* and *active* microrheology techniques using optical tweezers to estimate the mechanical properties of F-actin networks at a length scale comparable to cells. For the *passive* approach we tracked the motion of a thermally fluctuating colloidal sphere to estimate the frequency-dependent complex shear modulus of the network. In the *active* approach, we used an optical trap to oscillate an embedded microsphere and monitored the response to obtain network viscoelasticity over a physiologically relevant force range. While both *active* and *passive* measurements exhibit similar results at low strain, the F-actin network subject to high strain exhibits non-linear behavior which is analogous to the strain-hardening observed in macroscale measurements. Using confocal and TIRF microscopy, we also characterize the microstructure of reconstituted F-actin networks in terms of filament length, mesh size, and degree of bundling. Finally, we propose a model of network connectivity by investigating the effect of filament length on the mechanical properties and structure.

Keywords: F-actin network; shear modulus; α-actinin; filamin; gelsolin.

1. Introduction

Cells sense, generate and respond to forces in their environment through cytoskeletal dynamics, and mechanical force plays important roles in fundamental cellular processes such as migration, cytokinesis and apoptosis [1-3]. Actin, one of the principal constituents of the cytoskeleton, contributes to the mechanical integrity of the cell and is involved in numerous cellular functions organizing various microstructures according to functional demands [4,5]. Structural assembly of F-actin, critical in these processes, is regulated by over 100 actin binding proteins (ABPs) [6,7]. Two major structures of F-actin organized by ABPs are the cross-linked network and the bundled filament. For example, the ABP filamin assembles filaments into three-dimensional orthogonal networks serving as a scaffold for cell motility and signaling [8,9]; in contrast, α-actinin at high concentration forms thick bundles contributing to structural stability of the cell providing added mechanical strength [10,11]. Therefore, an understanding of cytoskeletal mechanical properties governed by dynamic interactions between actin and ABPs is essential for understanding cell mechanics and the associated biological phenomena.

Cell experiments have revealed that the cytoskeleton exhibits both elastic and viscous characteristics under applied stress [12,13]. Since it is difficult to accurately characterize the mechanical properties of the cytoskeleton *in vivo* due to active remodeling as well as the presence of numerous other, uncontrolled factors, *in vitro* experiments on re-constituted gels of F-actin have proven useful [14-19]. *In vitro* studies have characterized the viscoelastic properties of F-actin polymerized from purified actin in combination with various ABPs. Many of these measurements of mechanical properties have been performed using a bulk rheometer, which yields global properties of the F-actin matrix. Discrepancies have been observed, however, between these large length scale measurements and microrheometry using micron-scale beads

[20]. These have been attributed to a variety of factors including the non-uniform local stress field, different deformation modes [21], the formation of a depletion zone around the microbead [22,23], and other effects present when the bead is comparable in size to the characteristic dimensions of the actin mesh and individual actin filaments, both of which tend to be on the scale one to several microns [24]. While this similarity of length scales complicates interpretation of the results of microrheometry, it also provides an opportunity to probe the local mechanical response and provide insight into the specific roles of ABP in mediating rheological behavior. Other *in vitro* experiments have demonstrated that actin gels stiffen with increasing strain up to a point, then rapidly soften as strain is further increased [15,25-29]. Actin networks under shear deformation exhibit an irreversible non-linear behavior suggesting network remodeling and rupture of network bonds [26]. However, compressive force imposed on a dendritic actin network results in reversible stress softening suggesting that it might be caused by a different mechanism such as filament buckling [27]. The mechanisms for both the increase and sudden fall in modulus remain a subject of debate. Although models to explain these findings of actin cytoskeleton have been proposed [19,27,30], observation of network's response at the microscale will undoubtedly help elucidate the origin of this non-linear behavior.

Here we employ both passive and active microrheology to measure mechanical properties at the microscale using optical tweezers. Optical tweezers-based microrheology provides the advantage of high-precision force control in the range of 0.1 ~ 100pN while simultaneously monitoring the motion of the bead with nanometer resolution [31]. Although this technique has been used to measure viscoelastic properties of fd viruses and micellar solutions [32,33], its application to study F-actin networks has been limited [34]. In our passive approach, we track the motion of a thermally fluctuating microbead to estimate the frequency dependent complex

shear modulus of the F-actin network over a frequency range of 10^{-1} ~ 10^{4} Hz. For the active approach, we apply a sinusoidal driving force to an embedded microbead and monitor its response to obtain the viscoelastic properties of the network. In particular, microscale non-linear behavior of F-actin network is demonstrated by performing the active measurement at large deformation.

We investigate the effect of ABPs on the mechanical properties of F-actin networks using both *passive* and *active* techniques. To correlate mechanical properties with structural geometry, both material properties and microstructure of the cross-linked F-actin network are probed as a function of ABP concentration. Confocal microscopy and total internal reflection fluorescent (TIRF) microscopy are used to visualize the F-actin networks organized with filamin, α-actinin, and gelsolin. Unique features of F-actin networks polymerized with each ABP are visualized and quantified in terms of mesh size and degree of bundling. Average length of actin filaments is varied using gelsolin to investigate how the length of individual filaments alters network formation and its mechanical properties. While previous rheological measurements on entangled F-actin solutions have demonstrated that particle thermal motions are more constrained as the length of filament increases and as mesh size decreases [16,35], to our knowledge, no comparable measurements have been reported in cross-linked F-actin networks. Based on our measurements, we propose a model to explain how the length of individual actin filaments influences connectivity of the cross-linked network and its elasticity.

2. Materials and Methods

2.1. Microspheres

Amino functionalized beads (2.73% solids, Polybead Amino Microspheres; Polysciences, Warrington, PA) 0.5 and 1 μm in radius, are coated with mPEG-NHS (5 kDa; Nektar, San Carlos, CA) to prevent protein absorption as described previously [36] with the following modifications. Stock beads (40 μL) are diluted with 200 μL of de-ionized water. This solution is spun down for 10 minutes at 14,000 rpm, supernatant is removed and the bead pellet is resuspended with 200 μL of methanol. Next, the bead solution is again centrifuged as described above, the supernatant is removed and the bead pellet is resuspended with 200 μL of 10 mg/mL PEG-NHS diluted in one part DMSO and four parts methanol. After gently mixing the bead solution for two hours at room temperature, the beads are stored at 4°C with continuous rotation to prevent aggregation by sedimentation. Beads are used within 6 months of preparation.

2.2. Reconstituted in vitro F-actin networks

Lyophilized actin monomers and α-actinin both from rabbit skeletal muscle are purchased from Cytoskeleton Inc (Denver, CO). Activity and purity of actin are tested with sodium dodecyl sulfate-polyacrylamide gel electrophoresis (SDS-PAGE). Polymerized actin filaments are separated from the non-polymerized G-actin by centrifugation at 100,000g for 40min [37] and both supernatant and pellets are loaded on a 9% [wt/vol] PAGE gel. Protein bands stained with Coomassie blue show that most of G-actin is polymerized into F-actin (Fig. 1A). Protein activity is confirmed by examining the geometry of polymerized actin filaments in the micrographs (Fig. 1B and C). Recombinant filamin-A is purified from Sf9 cell lysates [38] and recombinant human gelsolin is produced in *Escherichia coli* [39].

Actin monomers are diluted in fresh G-buffer (5 mM Tris-HCl, 0.2 mM $CaCl_2$, 0.5mM DTT, 0.2 mM ATP, pH 8.0) and incubated on ice for at least two hours. Gelsolin, filamin or α-actinin are gently mixed with the actin monomer, followed by the addition of PEG-coated beads diluted in G-buffer. Actin polymerization is initiated by adding a tenth of the final volume of F-buffer (50 mM Tris-HCl, 500 mM KCl, 2 mM $MgCl_2$, 2 mM $CaCl_2$, 2 mM DTT, 5 mM ATP, 0.01% (w/v) NaN_3, pH 7.5). The sample is gently mixed by pipetting and immediately loaded into a custom-made flow chamber, with dimensions 25.8 mm x 8 mm x 0.1 mm (~ 20 μL). Microspheres are firmly embedded in the F-actin network after several hours of polymerization. Concentrations of actin, filamin, α-actinin, and gelsolin are varied depending on the experiment.

2.3. Characterizing F-actin microstructure

We visualize reconstituted F-actin structures polymerized with various ABPs and characterize them in terms of mesh size and degree of filament bundling . For visualization, fluorescently labeled actin (A-12373; Invitrogen, Carlsbad, CA) and rhodamine phalloidin (R415; Invitrogen, Carlsbad, CA) is used to stain actin filaments for confocal microscopy (Axiovert 200M; Carl Zeiss Inc., Thornwood, NY) and TIRF microscopy [40], respectively. In confocal microscopy, actin filaments are labeled by polymerizing regular actin monomers in the presence of labeled monomers at a molar ratio of 5:1. The sample is fixed by paraformaldehyde to minimize thermal fluctuations during image acquisition. A stack of 71 images is obtained with 100nm separation to obtain the three-dimensional (3D) structure. Images are then deconvolved with HUYGENS ESSENTIAL software (Scientific Volume Imaging, Hilversum, The Netherlands) and assembled to construct the 3D image by IMARIS software (Bitplane, Zurich, Switzerland). We characterize the mesh size of the actin networks from two-dimensional (2D) plane images, instead of the projected images, in order to minimize the misinterpretation from a projection of 3D structure.

Mesh size of the structure is determined by two methods. Each open area bounded by actin filaments is measured and mesh diameter (ξ) is given by $\xi = (4 \times Area/\pi)^{1/2}$. Mesh size is also estimated by measuring the peak-to-peak distance in the intensity profiles of the images. Corrections to these 2D measurements for three-dimensionality of the network are made according to Overby et al [41].

2.4. Experimental setup using optical tweezers

Optical tweezers-based microrheology is performed using a custom-built instrument described previously [40]. Briefly, a high numerical aperture objective (100X, 1.40 NA, oil IR; Nikon, Tokyo, Japan) tightly focuses a 1064-nm laser (Coherent, Santa Clara, CA) at the specimen plane for optical trapping. The trap location is computer-controlled with a pair of orthogonally oriented acousto-optic deflectors (AODs) (Intra-Action, Bellwood, IL) and sample positioning is controlled using a piezo-stage (Polytech PI, Auburn, MA) with nanometer resolution. The combination of a 975 nm laser (Corning, Corning, NY) and a position sensitive device (PSD) (Pacific Silicon, West Lake Village, CA) is employed for back-focal plane position detection [42]. The 975-nm laser is operated at ~ 0.1 mW such that it forms a negligible trap with respect to the 1064-nm laser operated between 5-100 mW. The detection zone consists of a circular area with radius of ~250 nm for 0.5 μm radius beads and ~500 nm for 1.0 μm beads. A second PSD is used to track the position of the trapping laser. The output voltages from both PSDs are collected by an A/D board (National Instruments, Austin, TX) and a custom program coded in LabView software (National Instruments, Texas, NI) is used to control experimental runs and data acquisition. Data analysis is performed using software written in MATLAB (Mathworks, Natick, MA).

Once the sample is loaded in the sample chamber and placed on the microscope stage, single beads are located and centered in the detection zone using an automated routine. After experimental runs (see below), the position of the bead is calibrated as described previously [43]. Optical tweezers were assumed to be a linear spring and the stiffness of the tweezers was characterized using free beads in buffer at different laser powers using standard calibration procedures [44].

2.5. Passive microrheology

Thermal fluctuations of an embedded bead, either 0.5 or 1.0μm in radius, are recorded at 50 kHz for ~42 seconds using the PSD. The complex compliance of the matrix, $\alpha(f)$, is computed from the power spectral density of the thermal motion using the fluctuation-dissipation theorem and the Kramers-Kronig relation [45]. The frequency-dependent complex shear modulus, $G(f)$, is determined by the generalized Stokes-Einstein relation, $G(f)=\left(6\pi a\alpha(f)\right)^{-1}$, where a is the radius of the bead. The storage shear modulus, $G'(f)$, and loss shear modulus, $G''(f)$, are the real and imaginary components of $G(f)$, respectively. We also acquire G by capturing and analyzing the time-evolution of the mean square displacement, $\langle \Delta r^2(t) \rangle$, [46].

2.6. Active microrheology

Sinusoidal force is applied to a microsphere embedded in the F-actin matrix by oscillating the optical tweezers using AODs. Amplitude of the sinusoidal excitation by the optical tweezers is set to ±200nm and frequency is varied from 0.1 to 10 Hz. Positions of both the optical tweezers and microsphere are detected by two separate PSDs simultaneously. We fit both the position of the trap, x_{trap}, and the position of the bead, x_{bead}, to sinusoidal functions of the form

$A\sin(2\pi ft-\theta)$, where A is amplitude, t is time, f is frequency of the input sinusoidal function and θ is the phase of each signal. The force, $F(t)$, exerted on the matrix is computed using

$$F(t)=k_{trap}\left[x_{trap}(t)-x_{bead}(t)\right], \tag{1}$$

where k_{trap} is the stiffness of the optical trap.

Since deformation of the matrix is given by x_{bead}, the frequency-dependent viscoelastic modulus is computed at a given frequency using

$$G(f)=G'(f)+iG''(f)=\frac{\bar{F}(f)}{6\pi a\bar{x}_{bead}(f)}\left[\cos(\Delta\theta(f))+i\sin(\Delta\theta(f))\right], \tag{2}$$

where $\bar{F}$ is the force amplitude, $\bar{x}_{bead}$ is the amplitude of the bead response and $\Delta\theta$ is the phase delay between $F(t)$ and $x_{bead}(t)$.

To impose large strain to the sample in the active measurement method, an optical tweezers is used to trap an embedded microsphere of a = 0.5 μm while moving the sample relative to the trap. The stage is moved sinusoidally with amplitudes of 400nm, 800nm and 1600nm at a frequency of 10Hz. We monitor the response of the microsphere and fit it to a sinusoidal function. Applied force is calculated from the distance of the microsphere from the center of the optical trap and k_{trap}. Network displacement is determined by calculating the difference between bead and stage displacements.

3. Results

3.1. Microstructures of F-actin networks

F-actin gels are prepared by polymerizing actin with filamin, α-actinin and gelsolin ([actin]/[gelsolin] = 250). They are visualized by confocal microscopy as described in Materials and Methods to investigate effects of cross-linking and bundling on F-actin network microstructure. For F-actin networks cross-linked with filamin, homogeneous networks are obtained over a range of the ratio of filamin to actin concentration (R_f) between 0.001 and 0.01 at a fixed actin concentration of 10μM (Fig. 2A). When R_f < 0.0001, F-actin networks form an inhomogeneous structure with large local variations, which is similar to the heterogeneity observed in F-actin networks cross-linked with low concentrations of heavy meromyosin [47]. When R_f > 0.01, the high concentration of filamin causes filament bundling and homogeneity of the network structure decreases consequently, as has also been reported in Goldmann et al [48]. F-actin networks with R_f = 0.01 (Fig. 2A) exhibit nearly orthogonal branchings where actin filaments are cross-linked (Fig. 2B). For F-actin organized by α-actinin, as the relative concentration of α-actinin (R_α) to the fixed concentration of actin (C_A = 10μM) increases, the degree of bundling increases as indicated by an increase in the relative fluorescent intensity of the filaments in confocal images (Fig. 2C). While a relatively homogeneous network is observed at low concentrations (R_α < 0.2), actin filaments form thick bundles at higher concentrations making the F-actin/α-actinin structure inhomogeneous. In the magnified image (Fig. 2D) for R_α = 0.2 (Fig. 2C), embedded bundles of actin filaments stand out compared to the smaller surrounding actin filaments. F-actin/filamin networks are characterized in terms of their mesh size, an important parameter in determining network mechanical properties. Mesh sizes for the homogeneous F-actin/filamin networks at both R_f = 0.001 and R_f = 0.01 are ~1μm (Figs. 3A and

B), which is similar in value to the mesh size in a previous study of F-actin/scruin networks [49]. As expected, the mesh size of a cross-linked network is determined by the concentration of actin, and is relatively independent of the ABP concentration. In contrast, mesh size of F-actin/α-actinin networks increases with the concentration of α-actinin (Figs. 3C and D). As more filament bundles are formed with increasing R_α, bundling by α-actinin increases the mesh size of the F-actin network. The increase in degree of filament bundling is seen as an increase in normalized filament intensity (Fig. 3E).

3.2. Mechanical properties of F-actin networks

Mechanical properties of the F-actin networks are estimated by passive and active methods. For C_A = 10μM and R_f = 0.01, the frequency dependent shear modulus is estimated by the passive measurement using the compliance function (Fig. 4A). At low frequency, G' dominates over G'' and approaches a constant value. At high frequency, $G'' > G'$ and G' scales as $f^{0.75}$ (Fig. 4A). Active measurements were performed at low amplitude, ±200nm, for the same F-actin/filamin network. The mechanical responses of the microsphere to sinusoidal excitation have different phase delays and amplitudes depending on excitation frequency (See Fig. 4B). As frequency increases, viscous dissipation increases as indicated by the large hysteresis in the curves (Fig. 4B). Values for shear modulus of the F-actin network, calculated at each frequency (Fig. 4C) using Eq. (2), are in good agreement with the result by passive measurement in Fig. 4A. To investigate the effects of large strain, active measurements were performed over a range of amplitudes. As the displacements increase, the response becomes non-linear as indicated by distortion of the force response (Fig. 5A) and the Lissajous curves (Fig. 5B). However, this microscale non-linear behavior is weak compared to the significant increase of modulus by strain-hardening observed in the bulk measurements [15,19]. In all other measurements of the

mechanical properties, we set the excitation amplitude at a low level (±200nm) to avoid nonlinear effects.

The effect on mechanical properties of cross-linking with filamin was studied both actively and passively at C_A = 10μM. As filamin concentration is increased from R_f = 0.01 to 0.04, both G' and G'' increase over the entire frequency range (Fig. 6A). Elastic effects become more dominant; relaxation frequency of the network (f_r), defined as the frequency when $G'(f_r) = G''(f_r)$, increases 23 fold as R_f increases four times. Complex shear moduli obtained by active and passive measurements are similar (Fig. 6B). The plateau storage shear modulus, G_0, estimated as that at the minimum value in G'' over the range of frequencies tested, also increases 14 fold as R_f increases.

3.3. Effect of filament length on network elasticity and structure

We next investigated the effect of mean filament length on mechanical properties and microstructure of the cross-linked F-actin networks polymerized at C_A = 10μM, R_f = 0.01 and in the presence and absence of gelsolin to regulate filament length. In the addition of gelsolin, the molar ratio of gelsolin to actin was 1:1000. To quantify the effect of gelsolin on filament length, we visualized single actin filaments polymerized in the presence and absence of gelsolin. While some long filaments are observed in the TIRF image for the actin polymerized in the absence of gelsolin (Fig. 7A), the addition of gelsolin decreases the lengths of the filaments significantly (Fig. 7B). Measurements from such micrographs show the average filament length to be 8.2 ± 5.2 μm and 2.2 ± 1.4 μm for the actin filaments polymerized in the absence and presence of gelsolin, respectively (Figs. 7C and D). Cross-linked F-actin networks organized by actin filaments with different average lengths were also visualized. TIRF images show that actin filaments in networks polymerized without gelsolin (Fig. 8A) are much longer than those in

networks polymerized with gelsolin (Fig. 8B). In the confocal images too, long filaments are observed only in the network without gelsolin (Fig. 8C). Mesh sizes in the network appear to be independent of gelsolin, and therefore, independent of the length of the actin filaments forming the network (Figs. 8E and F). However, both G' and G'' measured passively decrease as the length of actin filaments decreases (Fig. 8G). Plateau values seen in the MSD curves (*inset* in Fig. 8G) suggest that greater steric and elastic constraints are imposed in networks polymerized with longer actin filaments. The relaxation times ($= f_r^{-1}$) are approximately 0.2 sec for both short- and long-filament networks. Mechanical properties measured by the active method exhibit similar behavior having comparable values of both G_0 and f_r (Fig. 8H).

Networks were also probed using microspheres with a = 1 μm. With the large microspheres as well, both G' and G'' measured by the active method agrees well with corresponding values obtained with passive rheology. Agreement between the two methods does not depend on the average length of filaments as compared in Figs. 9A (no gelsolin) and 9B (with gelsolin). Relaxation times for both networks are similar, ~1 sec, but larger than the 0.2 sec relaxation time found in measurements with the smaller microsphere, a = 0.5μm. G_0 decreases as the average length of actin filament decrease (Fig. 9C). Although there is a discrepancy in G_0 between measurements made with a = 0.5 μm and a = 1 μm, G_0 of the network without gelsolin is higher than that with gelsolin indicating that, when the network is formed by long filaments, fluctuations of the embedded microsphere are more confined.

4. Discussion

In these experiments, we investigated the effects of actin filament length, method of measurement (active vs. passive and small vs. large probe), degree of cross-linking, and strain amplitude on the frequency-dependent shear moduli of reconstituted actin gels using a carefully characterized system. Other studies have typically reported the effects of these parameters individually, and few have studied the effect of filament length and strain-dependent rheology at the microscale. In addition, because minor differences in experimental protocol can lead to significant effects on measured moduli, we felt that it would be useful to have one complete set of measurements examining these multiple effects in a single system under tight control.

Passive and active microrheology produce similar results for F-actin networks, provided the strains are small and in the linear regime. We employed two complementary methods to measure gel microrheology. In the passive approach, frequency–dependent complex modulus was obtained over four decades in frequency by tracking thermal fluctuations of microspheres embedded in F-actin networks. The F-actin networks exhibit a plateau modulus (G_0) and a low G'' indicative of solid-like behavior at low frequencies. However, at high frequencies, G' exhibits a significantly greater frequency-dependence compared to the weak power law observed in cells [13,50]. In active measurements, the complex shear modulus is estimated by monitoring the mechanical response to the external force imposed by optical tweezers. Previous studies showed that actin and myosin networks exhibit different viscoelastic responses when measured by the active method compared to the passive method, which was attributed to tension in the filaments induced by myosin [34]. Since our system lacks motor proteins and applied strains are small and in the linear response range, the active and passive results show good agreement for our cross-linked F-actin networks. To a varying degree depending on measurement methods, the

mechanical moduli (G' and G'') of the *in vitro* F-actin networks tend to be smaller than those obtained from some measurements of living cells [12,13,51]. This difference has been attributed to the internal stresses in living cells arising from acto-myosin contraction, external adhesion, and potentially to the complexity of the cytoskeletal structure with the wide variety of ABPs found in a cell [34,51]. It is also important to note that our approaches are limited in that they probe local mechanical properties by monitoring the motion of a single particle. Single particle microrheology can be sensitive to the local environment of the embedded particle and the degree to which the particle is coupled to the matrix. Two-point microrheology overcomes these limitations by measuring the correlated motion of two particles [52]. As the length scale in the correlated motion is much larger than the size of the particle, two-point microrheology better reflects the bulk mechanical properties.

Employing the active measurement method, we are able to observe the microscale non-linear behavior of a cross-linked F-actin network. When loading amplitude is increased, in the present experiment by increasing the amplitude of stage oscillation, the force response of an F-actin network becomes non-linear resulting in a distortion of the Lissajous figures (Fig. 5B). This strain-dependent non-linear behavior at the microscale is qualitatively analogous to the mechanical properties of reconstituted actin gels under prestress probed at the macroscale [15,26,27] in that G' is observed to increase as the bead amplitude increases. However, the non-linearity observed in the present measurements is considerably smaller. The difference can be attributed to several factors. It should be noted that the strain and stress estimated here are not the differential values which has been measured in the macroscopic measurement with prestress using a rheometer [15] , but rather, the total amounts in response to progressively larger sinusoidal oscillations of the bead. Also, in the macroscopic measurements, applied shear stress

produces a non-affine deformation of the cross-linked F-actin network [53,54] inducing extension in some actin filaments and compression in others. As the thermal undulation in the stretched filaments is reduced, network elastic modulus increases. By contrast, in our microscale measurements, local excitation using a probe particle deforms only nearby filaments within a characteristic distance comparable to the size of the probe particle. While the macroscale method estimates global properties by measuring the response of the entire network, active microrheology probes local, microscale mechanical properties at force levels in the physiological range. Therefore, our techniques can be applied to probe the characteristics of individual cross-links as studied in single molecule assays [55]. Further study of strain-dependent microrheology for F-actin networks cross-linked with other ABPs will provide a better understanding of the microscopic origin of non-linear behavior in the F-actin networks.

The effects of ABP concentration are similar at the microscale to previous macroscale measurements. As filamin concentration increases for a given concentration of actin, G_0 increases 14 times as R increases four times. This is approximately consistent with previous macroscale studies showing a scaling of $G_0 \sim R^{\beta}$, with typical exponent, β from 0.4 to 2 depending on the ABP used [17,18,49]. For example, a short and rigid ABP, scruin, has a scaling exponent of 2 and heavy meromyosin (HMM) follows the scaling $G_0 \sim R^{1.2}$. As the dependence of G_0 on R reflects the molecular characteristics of the ABP (e.g., molecular structure, binding affinity and degree of dimerization [18]), filamin would appear to behave in a manner more similar to scruin than to HMM. It should be noted, however, that scaling of the modulus as a function of actin binding protein varies depending on the magnitude of R [26,47]. For the pre-stressed and highly cross-linked actin networks, the moduli are remarkably insensitive to concentrations of actin and actin binding protein [15].

Elasticity of the F-actin network is influenced by the length of actin filaments constituting the network. Gelsolin, a severing and capping protein, was used to regulate the contour length of actin filaments [56] and mechanical properties of the network polymerized in the absence and presence of gelsolin were compared (Fig. 8). *In vitro*, F-actin polymerizes to contour lengths, L, of about 2 - 70μm with a mean length of 20μm [57] and the average length of actin filaments can be adjusted by the concentration of gelsolin [56]. The gelsolin concentration used in these experiments regulates L to be 2μm, consistent with Janmey et al [56]. The G_o of cross-linked F-actin networks formed in the absence of gelsolin is higher than that in the presence of gelsolin, similar to the behavior seen with entangled F-actin solutions [16,20]. However, the effect on G_0 of gelsolin is smaller for cross-linked F-actin networks than for entangled F-actin solutions. While the elastic response of F-actin solutions is dominated by the entanglement length, L_e, the elasticity of an F-actin network is determined by the distance between cross-link points, L_c. Assuming affine deformations, the plateau storage shear modulus G_0 of a cross-linked F-actin network can be described by [58]

$$G_0 \sim \frac{\kappa^2}{kT}\xi^{-2}L_c^{-3}, \tag{3}$$

where ξ is the mesh size, κ is the bending modulus of actin filament, k is Boltzmann's constant, and T is the absolute temperature. If the networks with filamin are mostly cross-linked with negligible bundling, κ and ξ should not change with filament length as confirmed by our confocal images (Fig. 2) and their characterizations (Fig. 3). L_c in Eq. 3 is determined by the concentration of cross-linking protein [17]. We note, however, that Eq. 3 does not account for the effects of filament length. When the actin filament length is much larger than the mesh size, most ABPs cross-link filaments at the intersection points forming a well-defined highly interconnected network. In contrast, if the length of actin filaments is comparable to or only

slightly greater than the mesh size, many loose ends exist, which contribute little to the overall stiffness of the network. (Imagine the filaments of Fig. 10(A) being cut at random locations.). Reducing the length of individual filaments leads to more loose ends in the network configuration thereby altering network connectivity. The resulting effect is a network that is less capable of withstanding stress, and therefore exhibits a smaller modulus. Our findings therefore suggest that the mechanical response of cross-linked actin networks to external force is affected by filament length, which affects network connectivity, as well as L_c. Network connectivity can be investigated by visualizing cross-linking proteins as well as actin filaments. We tried to obtain the images of cross-linkers in a 3D actin network using filamin conjugated with fluorescent dye. However, it was difficult to identify individual cross-linking proteins because of the high background signal and thermal fluctuations of actin network that prevented us from obtaining clear images.

The size of the probe particle also has an effect on measured network viscoelasticity. To further investigate the effects of characteristic length scales in F-actin network microrheology, mechanical properties of F-actin network were probed using a larger microsphere (a = 1 μm) and the results compared to those obtained with the smaller one (a = 0.5 μm). G_0 of the network with L = 20 μm is consistently higher than that with L = 2 μm, however, values of G_0 are approximately 2~3 fold lower when measured using the larger microsphere as compared to the smaller one (Fig. 9C). That is, the elastic modulus of the F-actin network probed by the tracer whose diameter is comparable to the length of actin filaments (and mesh size) is smaller than that measured by the probe tracer which is much smaller than the filament length. Interestingly, a significant transition in G_0 has been observed in entangled F-actin solutions when the average length of actin filaments is close to the diameter of the microsphere used in the measurements

[16,20], which could, in both cases, be attributable to a local depletion zone created in the vicinity of a probe tracer. In network formation, long actin filaments are depleted from the immediate vicinity of the microsphere through a combination of their high bending stiffness and steric exclusion. Therefore, the microsphere resides in an environment that is more viscous than elastic leading to a reduced G' but having little impact on G''. This is reflected in the observation that the larger microsphere exhibits a smaller relaxation frequency (f_r) at which $G' = G''$. Also the larger microsphere exhibits a scaling $G'' \sim f^{0.85}$ at high frequency indicating that the local environment behaves in a manner more reminiscent of a Newtonian fluid as compared to the scaling $G'' \sim f^{0.75}$ observed with $a = 0.5$ μm and $L = 20$ μm.

5. Conclusions

We employed methods of passive and active microrheology using optical tweezers and observed the mechanical properties of homogeneous F-actin networks. The microscale non-linear behavior of the cross-linked F-actin network was obtained by active measurement at high strain. The effects of length scale on both network elasticity and microstructure were investigated by controlling actin filament length and probe size. We showed that short actin filaments influence connectivity of the network structure resulting in a reduced elasticity. The results presented here and future similar studies with different actin-binding proteins will provide insight into the microscopic origin of mechanical properties in cross-linked F-actin networks.

Acknowledgements

We are grateful to T.P. Stossel for helpful discussions. This work was supported by the NIGMS (GM076689) (to H.L. and R.D.K.), the NSF Career Award (0643745) (to M.J.L.), the

Nicholas Hobson Wheeles, Jr. Fellowship (to J.M.F.), the W.M. Keck Foundation (to M.J.L.), the Westaway Research Fund (to M.J.L.), and the Singapore-MIT Alliance for Research and Technology.

References

1. Janmey PA, McCulloch CA. Cell mechanics: integrating cell responses to mechanical stimuli. Annu Rev Biomed Eng 2007; 9: 1-34.
2. Khan S, Sheetz MP. Force effects on biochemical kinetics. Annu Rev Biochem 1997; 66: 785-805.
3. Vogel V, Sheetz M. Local force and geometry sensing regulate cell functions. Nat Rev Mol Cell Biol 2006; 7: 265-275.
4. Bartles JR. Parallel actin bundles and their multiple actin-bundling proteins. Curr Opin Cell Biol 2000; 12: 72-78.
5. Stossel TP, Fenteany G, Hartwig JH. Cell surface actin remodeling. J Cell Sci 2006; 119: 3261-3264.
6. dos Remedios CG, Chhabra D, Kekic M, Dedova IV, Tsubakihara M, Berry DA, Nosworthy NJ. Actin binding proteins: regulation of cytoskeletal microfilaments. Physiol Rev 2003; 83: 433-473.
7. Pollard TD, Cooper JA. Actin and actin-binding proteins. A critical evaluation of mechanisms and functions. Annu Rev Biochem 1986; 55: 987-1035.
8. Stossel TP, Condeelis J, Cooley L, Hartwig JH, Noegel A, Schleicher M, Shapiro SS. Filamins as integrators of cell mechanics and signalling. Nat Rev Mol Cell Biol 2001; 2: 138-145.
9. Feng Y, Walsh CA. The many faces of filamin: a versatile molecular scaffold for cell motility and signalling. Nat Cell Biol 2004; 6: 1034-1038.
10. Meyer RK, Aebi U. Bundling of actin filaments by alpha-actinin depends on its molecular length. J Cell Biol 1990; 110: 2013-2024.
11. Wachsstock DH, Schwartz WH, Pollard TD. Affinity of alpha-actinin for actin determines the structure and mechanical properties of actin filament gels. Biophys J 1993; 65: 205-214.
12. Bausch AR, Moller W, Sackmann E. Measurement of local viscoelasticity and forces in living cells by magnetic tweezers. Biophys J 1999; 76: 573-579.
13. Fabry B, Maksym GN, Butler JP, Glogauer M, Navajas D, Fredberg JJ. Scaling the microrheology of living cells. Phys Rev Lett 2001; 87: 148102.
14. Claessens MMAE, Tharmann R, Kroy K, Bausch AR. Microstructure and viscoelasticity of confined serniflexible polymer networks. Nat Phys 2006; 2: 186-189.
15. Gardel ML, Nakamura F, Hartwig JH, Crocker JC, Stossel TP, Weitz DA. Prestressed F-actin networks cross-linked by hinged filamins replicate mechanical properties of cells. P Natl Acad Sci USA 2006; 103: 1762-1767.
16. Liu J et al. Microrheology probes length scale dependent rheology. Phys Rev Lett 2006; 96: 118104.
17. Tharmann R, Claessens MMAE, Bausch AR. Viscoelasticity of isotropically cross-linked actin networks. Phys Rev Lett 2007; 98: 088103.
18. Wagner B, Tharmann R, Haase I, Fischer M, Bausch AR. Cytoskeletal polymer networks: the molecular structure of cross-linkers determines macroscopic properties. P Natl Acad Sci USA 2006; 103: 13974-13978.
19. Xu JY, Tseng Y, Wirtz D. Strain hardening of actin filament networks - Regulation by the dynamic cross-linking protein alpha-actinin. J Biol Chem 2000; 275: 35886-35892.

20. Schmidt FG, Hinner B, Sackmann E. Microrheometry underestimates the values of the viscoelastic moduli in measurements on F-actin solutions compared to macrorheometry. Phys Rev E 2000; 61: 5646-5653.
21. Maggs AC. Micro-bead mechanics with actin filaments. Phys Rev E 1998; 57: 2091-2094.
22. Levine AJ, Lubensky TC. Two-point microrheology and the electrostatic analogy. Phys Rev E 2002; 65: 011501.
23. Morse DC. Viscoelasticity of concentrated isotropic solutions of semiflexible polymers. 2. Linear response. Macromolecules 1998; 31: 7044-7067.
24. Schmidt CF, Barmann M, Isenberg G, Sackmann E. Chain Dynamics, Mesh Size, and Diffusive Transport in Networks of Polymerized Actin - a Quasielastic Light-Scattering and Microfluorescence Study. Macromolecules 1989; 22: 3638-3649.
25. Gardel ML, Nakamura F, Hartwig J, Crocker JC, Stossel TP, Weitz DA. Stress-dependent elasticity of composite actin networks as a model for cell behavior. Phys Rev Lett 2006; 96: 088102.
26. Gardel ML, Shin JH, MacKintosh FC, Mahadevan L, Matsudaira P, Weitz DA. Elastic behavior of cross-linked and bundled actin networks. Science 2004; 304: 1301-1305.
27. Chaudhuri O, Parekh SH, Fletcher DA. Reversible stress softening of actin networks. Nature 2007; 445: 295-298.
28. Storm C, Pastore JJ, MacKintosh FC, Lubensky TC, Janmey PA. Nonlinear elasticity in biological gels. Nature 2005; 435: 191-194.
29. Janmey PA, Hvidt S, Lamb J, Stossel TP. Resemblance of Actin-Binding Protein Actin Gels to Covalently Cross-Linked Networks. Nature 1990; 345: 89-92.
30. Janmey PA, McCormick ME, Rammensee S, Leight JL, Georges PC, MacKintosh FC. Negative normal stress in semiflexible biopolymer gels. Nat Mater 2007; 6: 48-51.
31. Brau RR et al. Passive and active microrheology with optical tweezers. J Opt A-Pure Appl Opt 2007; 9: S103-S112.
32. Addas KM, Schmidt CF, Tang JX. Microrheology of solutions of semiflexible biopolymer filaments using laser tweezers interferometry. Phys Rev E 2004; 70: 021503.
33. Atakhorrami M, Schmidt CF. High-bandwidth one- and two-particle microrheology in solutions of wormlike micelles. Rheol Acta 2006; 45: 449-456.
34. Mizuno D, Tardin C, Schmidt CF, MacKintosh FC. Nonequilibrium mechanics of active cytoskeletal networks. Science 2007; 315: 370-373.
35. Wong IY, Gardel ML, Reichman DR, Weeks ER, Valentine MT, Bausch AR, Weitz DA. Anomalous diffusion probes microstructure dynamics of entangled F-actin networks. Phys Rev Lett 2004; 92: 178101.
36. Valentine MT, Perlman ZE, Gardel ML, Shin JH, Matsudaira P, Mitchison TJ, Weitz DA. Colloid surface chemistry critically affects multiple particle tracking measurements of biomaterials. Biophys J 2004; 86: 4004-4014.
37. Zuchero JB. In vitro actin assembly assays and purification from acanthamoeba. Methods Mol Biol 2007; 370: 213-226.
38. Nakamura F, Osborn E, Janmey PA, Stossel TP. Comparison of filamin A-induced cross-linking and Arp2/3 complex-mediated branching on the mechanics of actin filaments. J Biol Chem 2002; 277: 9148-9154.
39. Kwiatkowski DJ, Janmey PA, Yin HL. Identification of Critical Functional and Regulatory Domains in Gelsolin. J Cell Biol 1989; 108: 1717-1726.

40. Brau RR, Tarsa PB, Ferrer JM, Lee P, Lang MJ. Interlaced Optical Force-Fluorescence Measurements for Single Molecule Biophysics. Biophys J 2006; 91: 1069-1077.
41. Overby D, Ruberti J, Gong HY, Freddo TF, Johnson M. Specific hydraulic conductivity of corneal stroma as seen by quick-freeze/deep-etch. J Biomech Eng-Trans ASME 2001; 123: 154-161.
42. Gittes F, Schmidt CF. Back-focal-plane detection of force and motion in optical traps. Biophys J 1998; 74: A183-A183.
43. Lang MJ, Asbury CL, Shaevitz JW, Block SM. An automated two-dimensional optical force clamp for single molecule studies. Biophys J 2002; 83: 491-501.
44. Neuman KC, Block SM. Optical trapping. Rev Sci Instrum. 2004; 75: 2787-2809.
45. Chaikin PM, Lubensky TC. Principles of Condensed Matter Physics. Cambridge University Press. 1995.
46. Mason TG, Weitz DA. Optical Measurements of Frequency-Dependent Linear Viscoelastic Moduli of Complex Fluids. Phys Rev Lett 1995; 74: 1250-1253.
47. Luan Y, Lieleg O, Wagner B, Bausch AR. Micro- and macrorheological properties of isotropically cross-linked actin networks. Biophys J 2008; 94: 688-693.
48. Goldmann WH, Tempel M, Sprenger I, Isenberg G, Ezzell RM. Viscoelasticity of actin-gelsolin networks in the presence of filamin. Eur J Biochem 1997; 246: 373-379.
49. Shin JH, Gardel ML, Mahadevan L, Matsudaira P, Weitz DA. Relating microstructure to rheology of a bundled and cross-linked F-actin network in vitro. P Natl Acad Sci USA 2004; 101: 9636-9641.
50. Hoffman BD, Massiera G, Van Citters KM, Crocker JC. The consensus mechanics of cultured mammalian cells. P Natl Acad Sci USA 2006; 103: 10259-10264.
51. Wang N, Tolic-Norrelykke IM, Chen J, Mijailovich SM, Butler JP, Fredberg JJ, Stamenovic D. Cell prestress. I. Stiffness and prestress are closely associated in adherent contractile cells. Am J Physiol Cell Physiol 2002; 282: C606-616.
52. Crocker JC, Valentine MT, Weeks ER, Gisler T, Kaplan PD, Yodh AG, Weitz DA. Two-point microrheology of inhomogeneous soft materials. Phys Rev Lett 2000; 85: 888-891.
53. Head DA, Levine AJ, MacKintosh EC. Deformation of cross-linked semiflexible polymer networks. Phys Rev Lett 2003; 91: 108102.
54. Onck PR, Koeman T, van Dillen T, van der Giessen E. Alternative explanation of stiffening in cross-linked semiflexible networks. Phys Rev Lett 2005; 95: 178102.
55. Ferrer JM, Lee H, Chen J, Pelz B, Nakamura F, Kamm RD, Lang MJ. Measuring molecular rupture forces between single actin filaments and actin-binding proteins. P Natl Acad Sci USA 2008; 105: 9221-9226.
56. Janmey PA, Peetermans J, Zaner KS, Stossel TP, Tanaka T. Structure and Mobility of Actin-Filaments as Measured by Quasi-Elastic Light-Scattering, Viscometry, and Electron-Microscopy. J Biol Chem 1986; 261: 8357-8362.
57. Kaufmann S, Kas J, Goldmann WH, Sackmann E, Isenberg G. Talin anchors and nucleates actin filaments at lipid membranes. A direct demonstration. FEBS Lett 1992; 314: 203-205.
58. Mackintosh FC, Kas J, Janmey PA. Elasticity of Semiflexible Biopolymer Networks. Phys Rev Lett 1995; 75: 4425-4428.

Figure legends

Fig. 1. Characrerization of actin. (A) Scanned image of the polyacrylamide gel. Lane #1, G-actin kept overnight on ice, #2, G-actin after centrifuge without polymerization, #3, supernatant after centrifugation of polymerized actin, and #4, pellet after centrifugation of polymerized actin. Bands observed in lane #1 and #2 confirmed that actin is in monomeric form in G-buffer. In contrast to lane #4, no protein band is observed in lane #3 suggesting that most of the G-actin monomers are polymerized into F-actin during polymerization. (B) Electron microscope image of F-actin which are negatively stained with 2% uranyl acetate (scale bar, 200nm). *Inset*: The diameter of actin filament is measured to be approximately 6nm. (C) TIRF microscopy shows that the length of polymerized actin filaments are varying over 20 μm (scale bar, 5μm).

Fig. 2. Confocal microscopy of F-actin organized by actin binding proteins. Images are projections of 71 layers each separated by 100nm. (A) Confocal images of F-actin cross-linked with two different concentrations of filamin (scale bar, 10μm). In a limited range of R_f between 0.001 and 0.01, the cross-linked F-actin networks exhibit uniform and fine microstructures. (B) Higher magnification of a single layer image for F-actin cross-linked by filamin with R_f = 0.01 (scale bar, 5μm). The image shows filamin forming F-actin cross-links at high angle. *Inset*: Magnification of the orthogonal cross-linking point. (C) Confocal images of F-actin organized with various concentrations of α-actinin (scale bar, 10μm). Degree of bundling increases as the concentration of α-actinin increases relative to the concentration of actin. *Inset*: Magnification of the actin filament bundles. (D) Higher magnification image of filaments with R_α = 0.02 showing the evolution toward more highly bundled filaments (scale bar, 5μm).

Fig. 3. Microstructural characterizations. Mesh sizes computed from the mesh area (orange) and the peak-to-peak distance (blue) in the images. 3D mesh size (green) is estimated using the properties of 2D meshes. (A) Distributions of mesh size, ξ, in the F-actin networks cross-linked with filamin at various R_f. (B) Mean and standard deviation of mesh size plotted against R_f. (C) Distributions of mesh size, ξ, in the F-actin networks organized by α-actinin at various R_α. (D) Mean and standard deviation of the mesh size plotted against R_α. As R_α increases, more filament bundles are formed and the mesh size of the networks increases. (E) Distributions of normalized intensity of the filaments in the F-actin networks at various R_α.

Fig. 4. Frequency-dependent mechanical properties in passive and active microrheology for F-actin networks with C_A = 10μM at R_f = 0.01. (A) Passive measurements; the complex shear moduli G' (circles) and G'' (squares) of F-actin networks are estimated over 4 decades of frequency by tracking the thermal fluctuations of an embedded microsphere. Solid line has a slope of 0.75. *Inset*: MSD of the microsphere. (B) Active measurements; a sinusoidal forcing applied to an embedded microsphere using optical tweezers. As the frequency increases, viscous dissipation increases as seen by a wider hysteresis in the force vs. bead displacement plot. *Inset*: sample traces of the position of the trapping laser (thick solid line) and the responses of a microsphere for 0.5Hz (thin solid line) and 5Hz (dotted line) excitation frequencies. (C) Storage (circle) and loss (square) moduli of F-actin network obtained using the active approach.

Fig. 5. Mechanical behavior of cross-linked F-actin network subject to large oscillatory deformation. Symbols in the figures correspond to the applied deformation: 400nm (.....), 800nm (- - -), and 1600 nm (—). (A) Force versus time. The amplitude of force increases as the applied deformation increases. As indicated by the distortions in the force curves, the network exhibits a non-linear response at large deformation. (B) Corresponding Lissajous figure. The ellipse-shape Lissajous curve is deformed by the non-linear behavior at large deformation.

Fig. 6. Effect of cross-linker fractional concentration, R_f, on complex shear modulus. Storage and loss shear moduli are estimated for C_A = 10μM at R_f = 0.01 (open) and R_f = 0.04 (closed). G' (circle) and G'' (square) by passive method, G' (diamond) and G'' (triangle) by active method. In both passive (A) and active (B) measurements, shear moduli increase as R_f increases.

Fig. 7. Effect of gelsolin on filament length. Micrographs show that actin filaments polymerized in the absence of gelsolin (A) are much longer than those in the presence of gelsolin (B). Length distributions for both conditions are obtained by measuring the length of single actin filaments from micrographs (C, D).

Fig. 8. Effect of gelsolin on microstructure and microrheology of F-actin network. TIRF (A,B) and confocal microscopy (C,D) images of F-actin/filamin network polymerized in the absence (A,C) and presence (B,D) of gelsolin (scale bar, 10μm). Although longer actin filaments are observed in the F-actin network polymerized in the absence of gelsolin, the mesh size distributions obtained by two different methods (see text for details) are similar for the network without gelsolin (E) and the network with gelsolin (F). Frequency dependent shear moduli of F-actin networks without gelsolin (open symbols) and with gelsolin (closed symbols) are measured using passive (G) and active (H) methods. G' (circle) and G'' (square) by passive method, G' (diamond) and G'' (triangle) by active method. The moduli obtained from the two methods exhibit similar results. Both G' and G'' are higher for the F-actin network polymerized in the absence of gelsolin (longer filaments) over the entire frequency range. *Inset* in (G): MSD curves for the F-actin networks in the presence (dotted) and absence (solid) of gelsolin.

Fig. 9. Effects of probe size, filament length and measurement method on microrheology of cross-linked F-actin networks. Using a larger microsphere with radius a = 1μm, the complex shear moduli are estimated for the F-actin networks polymerized in the absence (A) and presence (B) of gelsolin. G' (circle) and G'' (triangle) by passive (blue) and active (orange) methods. Both passive and active measurements exhibit similar results independent of filament length. (C) Comparison of G_0 obtained by passive (blue circles) and active (orange triangles) measurements for the F-actin network with and without gelsolin. F-actin networks formed with short filaments are less stiff than those formed with long filaments. The decrements in G_0 are similar, independent of the microsphere's dimension (solid: a = 0.5μm; dotted: a = 1μm).

Fig. 10. Schematic illustrations of F-actin network organized by long (A) and short (B) actin filaments at identical concentrations of actin filaments and cross-linkers. In the network with long filaments (A), most filaments are attached at each crossing point by ABPs that are arranged regularly along the filaments. In contrast, the network with short filaments (B) forms incomplete loops with many loose ends, and their arrangement is random compared to the network in (A). This difference in structure would cause the network with short filaments to be less stiff than the one with long filaments.

Figures

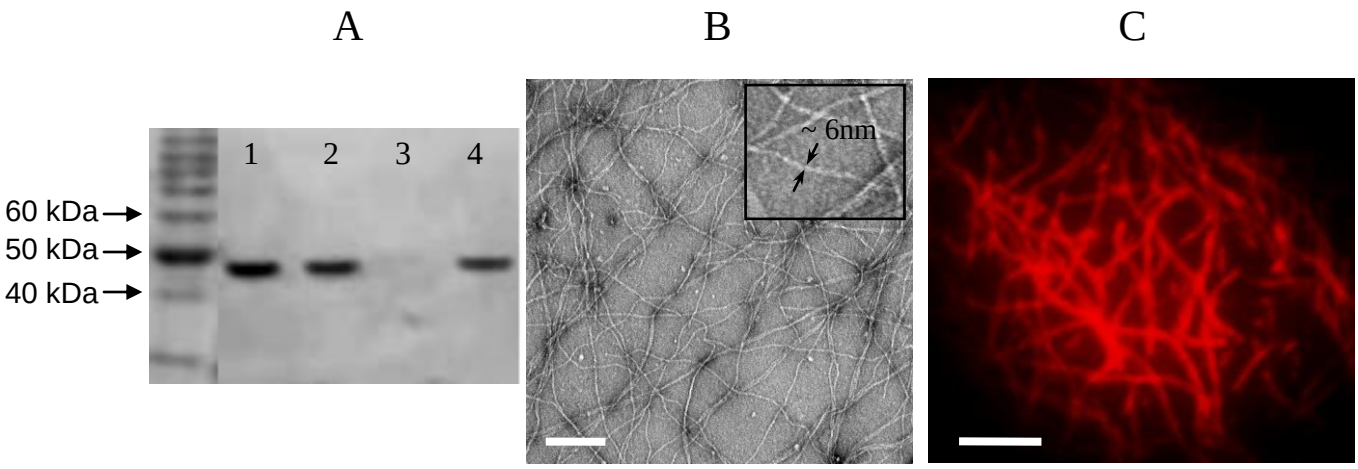

Fig. 1

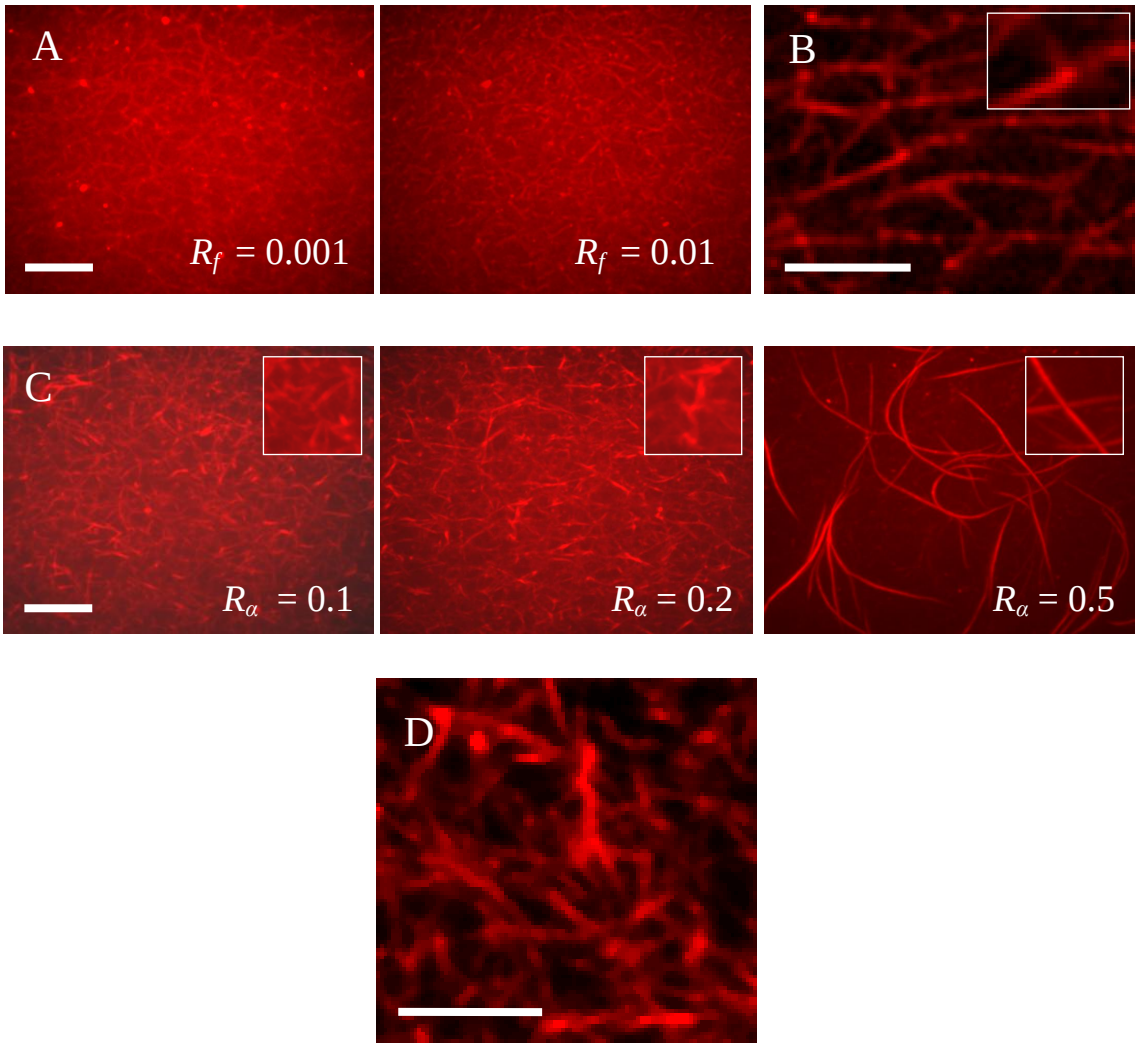

Fig. 2

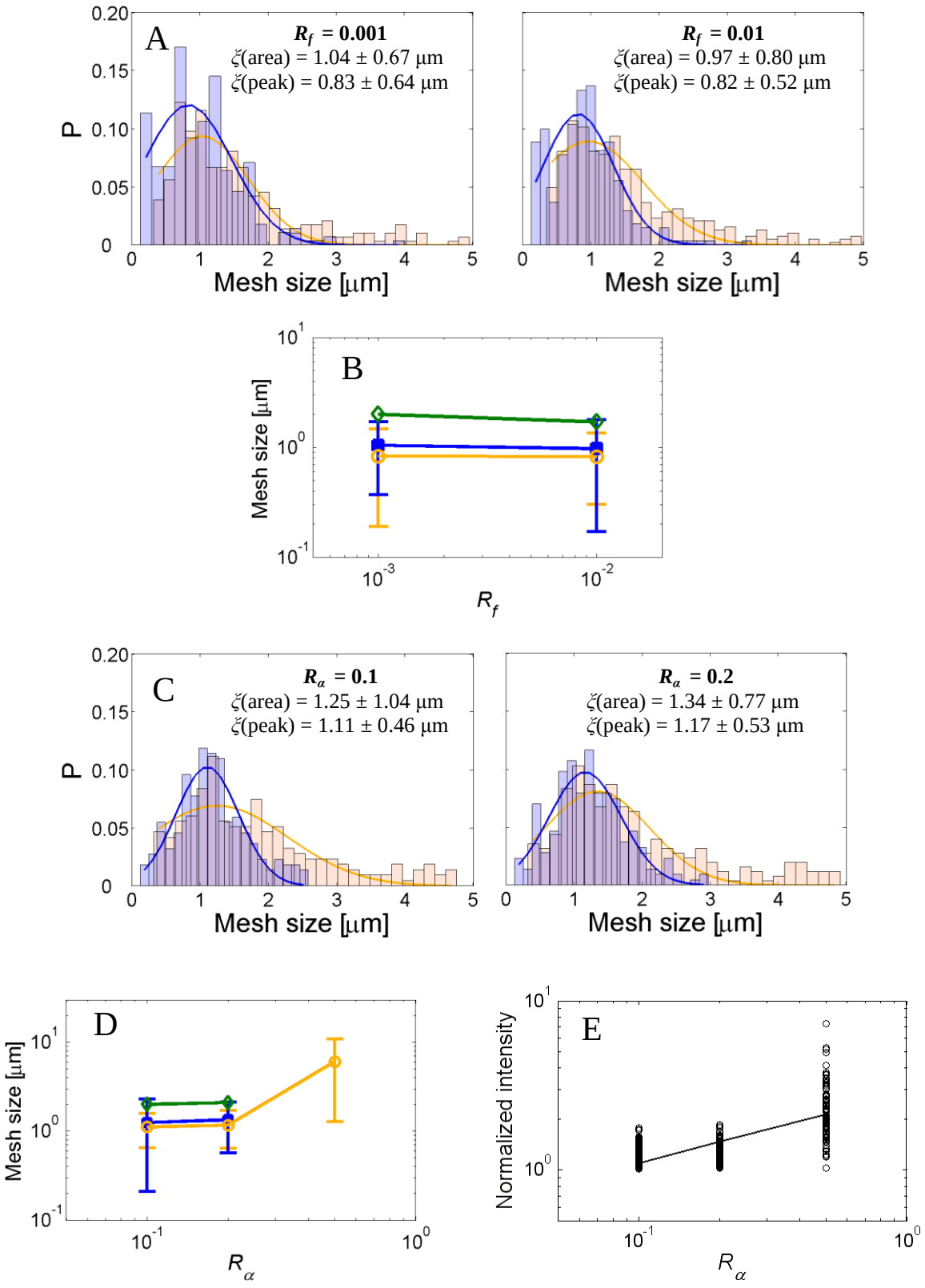
A
R_f = 0.001
ξ(area) = 1.04 ± 0.67 μm
ξ(peak) = 0.83 ± 0.64 μm
R_f = 0.01
ξ(area) = 0.97 ± 0.80 μm
ξ(peak) = 0.82 ± 0.52 μm
P
Mesh size [μm]
B
Mesh size [μm]
R_f
C
$R_α$ = 0.1
ξ(area) = 1.25 ± 1.04 μm
ξ(peak) = 1.11 ± 0.46 μm
$R_α$ = 0.2
ξ(area) = 1.34 ± 0.77 μm
ξ(peak) = 1.17 ± 0.53 μm
D
E
Normalized intensity
$R_α$

Fig. 3

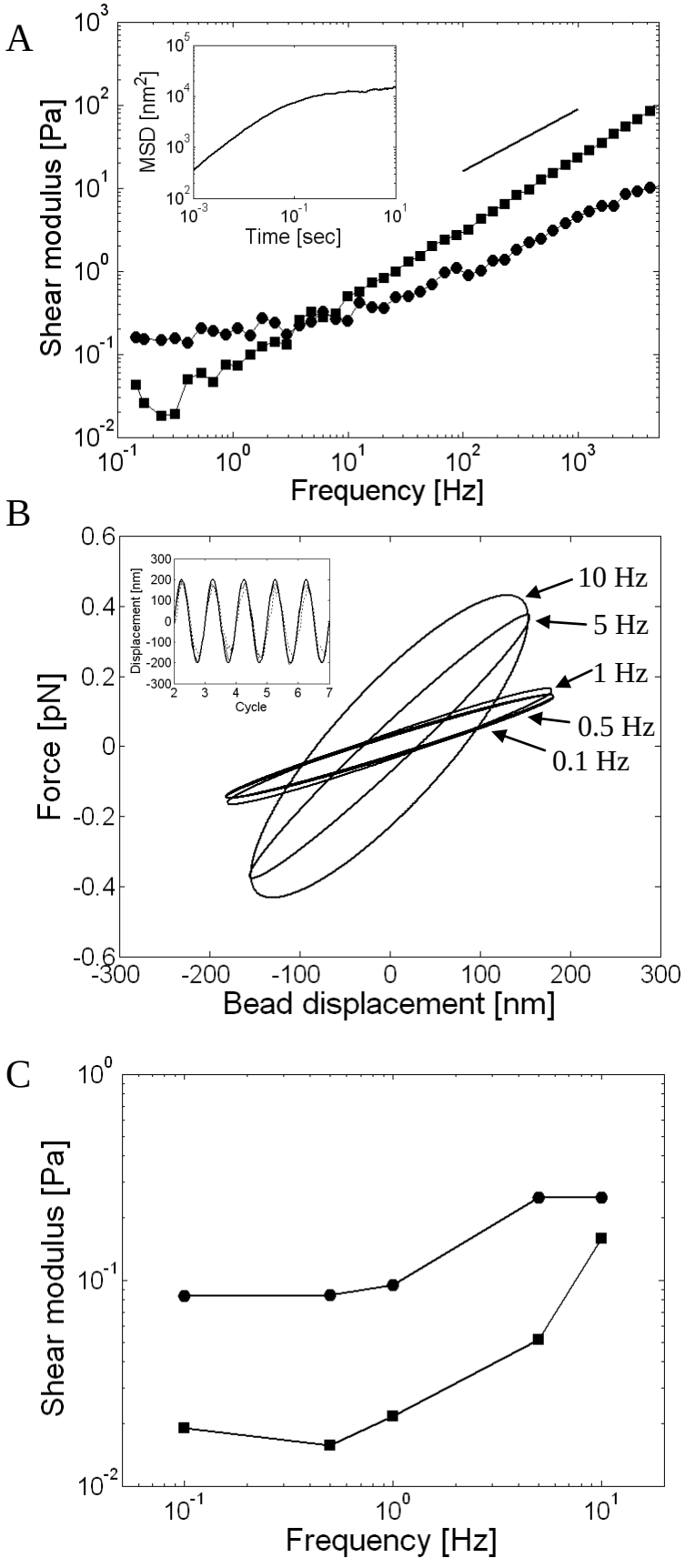
A
Shear modulus [Pa]
Frequency [Hz]
MSD [nm²]
Time [sec]
B
Force [pN]
Bead displacement [nm]
Displacement [nm]
Cycle
10 Hz
5 Hz
1 Hz
0.5 Hz
0.1 Hz
C
Shear modulus [Pa]
Frequency [Hz]

Fig. 4

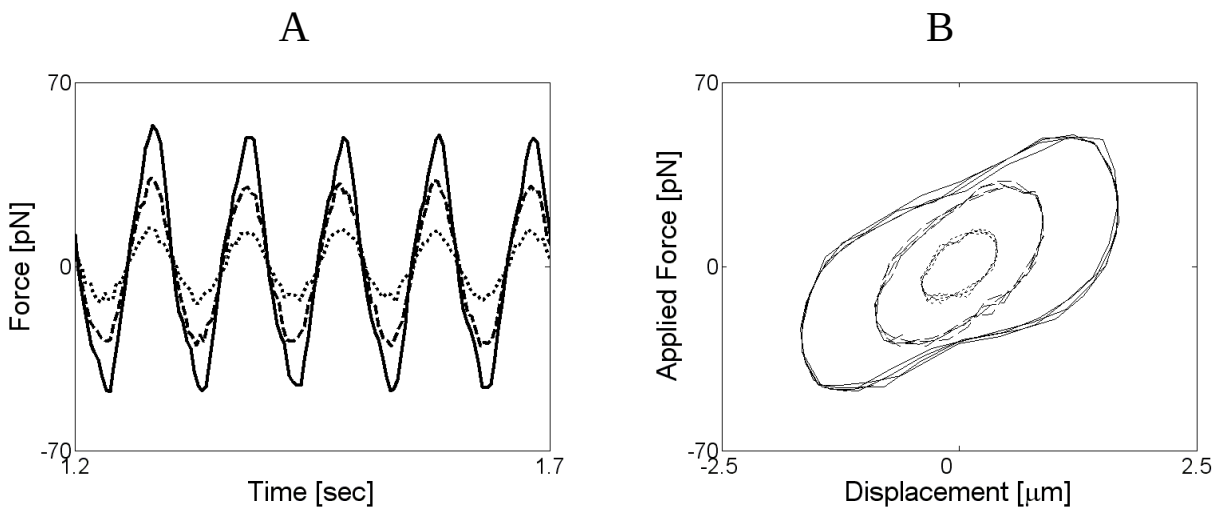
A
B
70
0
-70
Force [pN]
1.2
1.7
Time [sec]
70
0
-70
Applied Force [pN]
-2.5
0
2.5
Displacement [μm]

Fig. 5

A

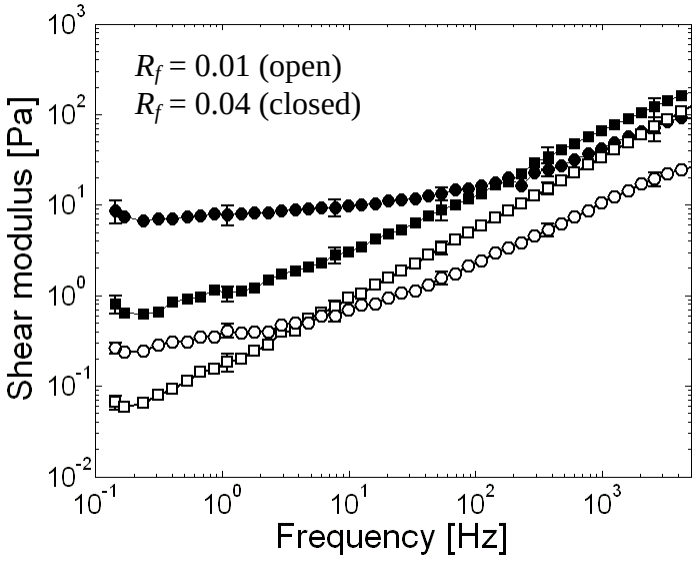
R_f = 0.01 (open)
R_f = 0.04 (closed)
Shear modulus [Pa]
Frequency [Hz]

B

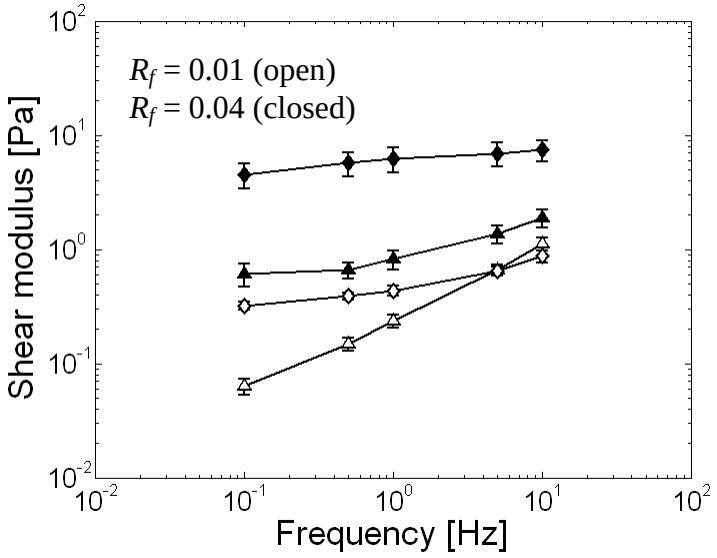
R_f = 0.01 (open)
R_f = 0.04 (closed)
Shear modulus [Pa]
Frequency [Hz]

Fig. 6

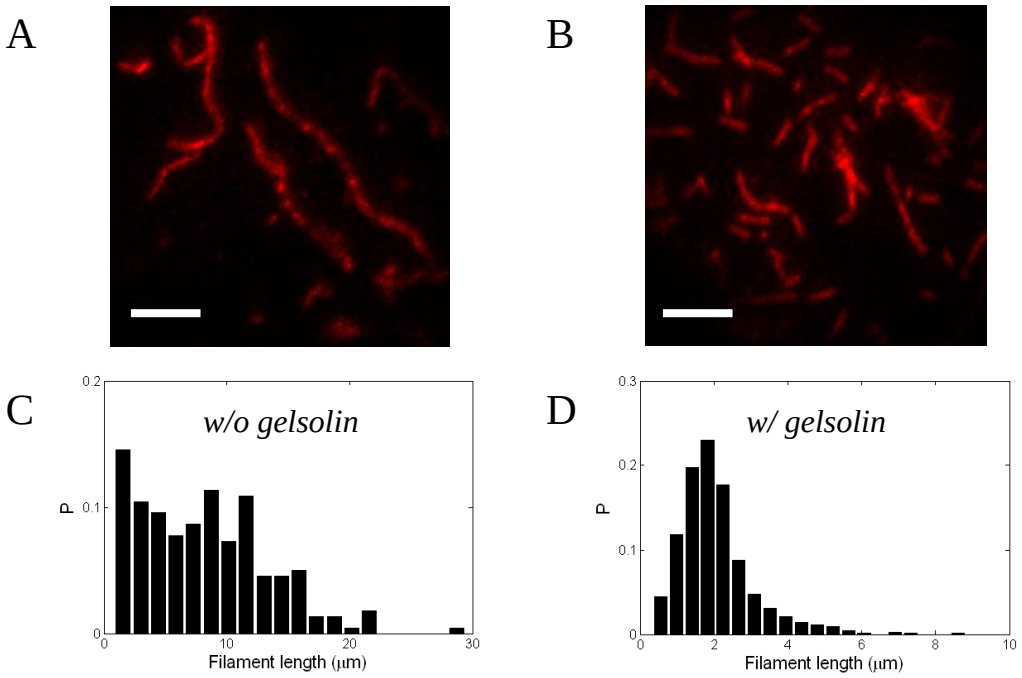
A
B
C
D
w/o gelsolin
w/ gelsolin
P
Filament length (μm)
0
0.1
0.2
10
20
30
0.3
2
4
6
8

Fig. 7

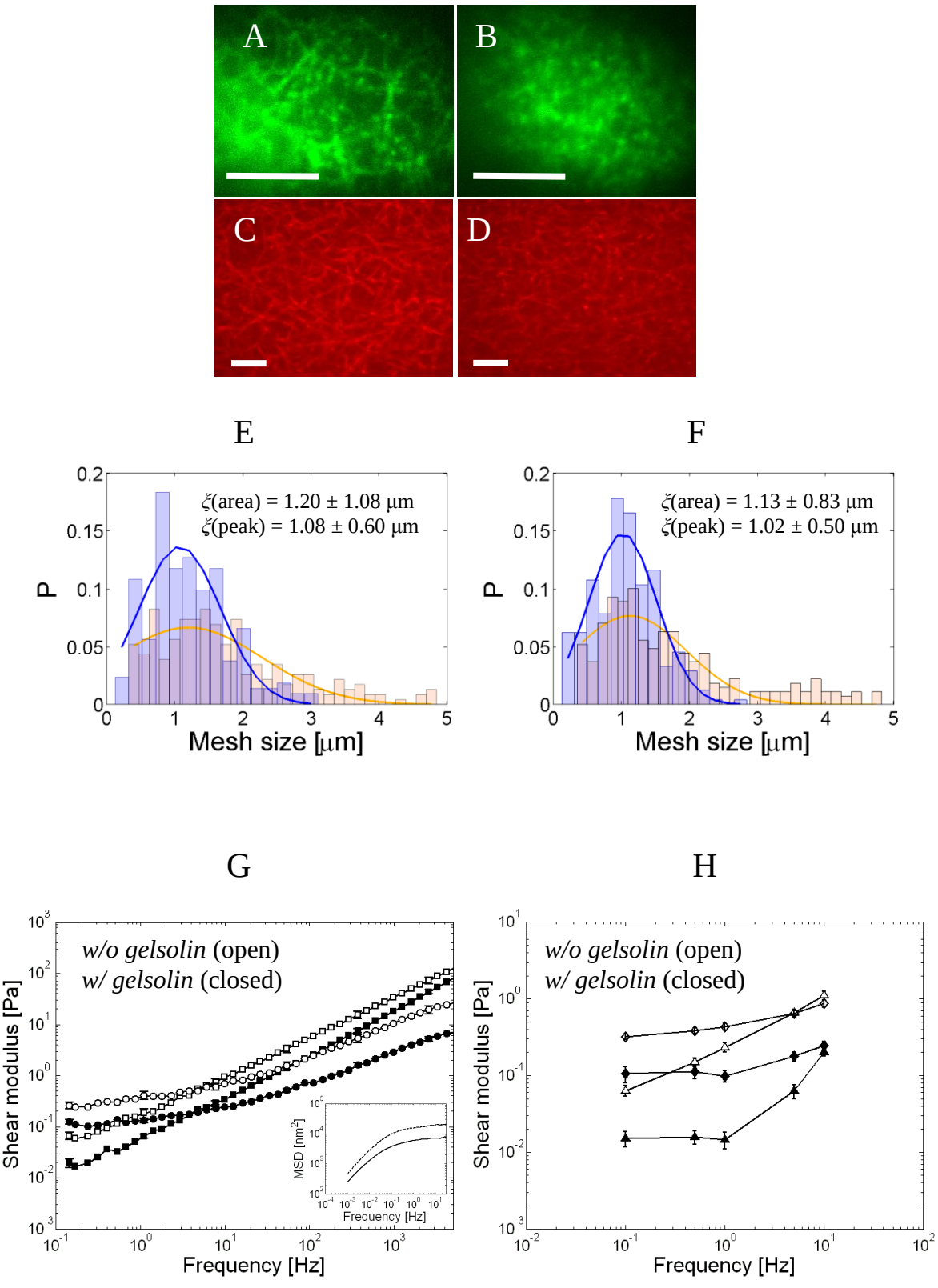
A
B
C
D
E
F
ξ(area) = 1.20 ± 1.08 μm
ξ(peak) = 1.08 ± 0.60 μm
P
Mesh size [μm]
ξ(area) = 1.13 ± 0.83 μm
ξ(peak) = 1.02 ± 0.50 μm
P
Mesh size [μm]
G
H
w/o gelsolin (open)
w/ gelsolin (closed)
Shear modulus [Pa]
Frequency [Hz]
MSD [nm²]
Frequency [Hz]
w/o gelsolin (open)
w/ gelsolin (closed)
Shear modulus [Pa]
Frequency [Hz]

Fig. 8

A

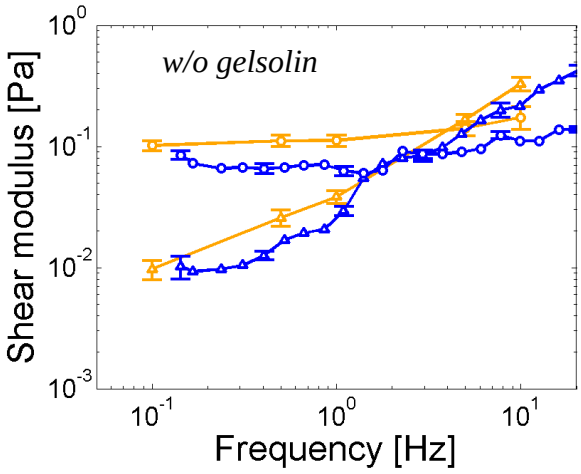
w/o gelsolin
Shear modulus [Pa]
Frequency [Hz]
10^0
10^-1
10^-2
10^-3
10^-1
10^0
10^1

B

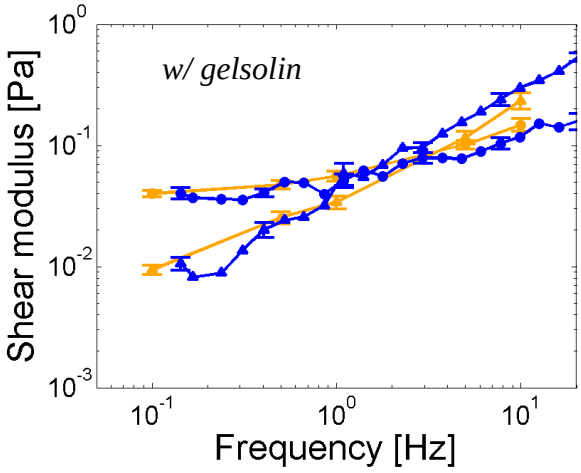
w/ gelsolin
Shear modulus [Pa]
Frequency [Hz]
10^0
10^-1
10^-2
10^-3
10^-1
10^0
10^1

C

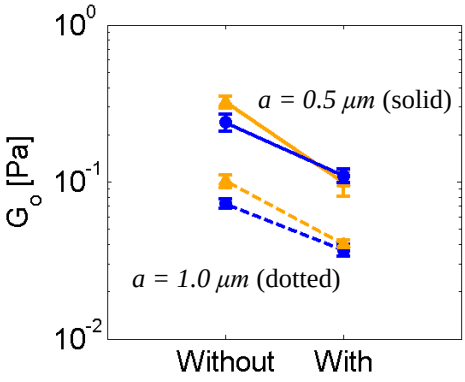
a = 0.5 μm (solid)
a = 1.0 μm (dotted)
G_o [Pa]
10^0
10^-1
10^-2
Without
With

Fig. 9

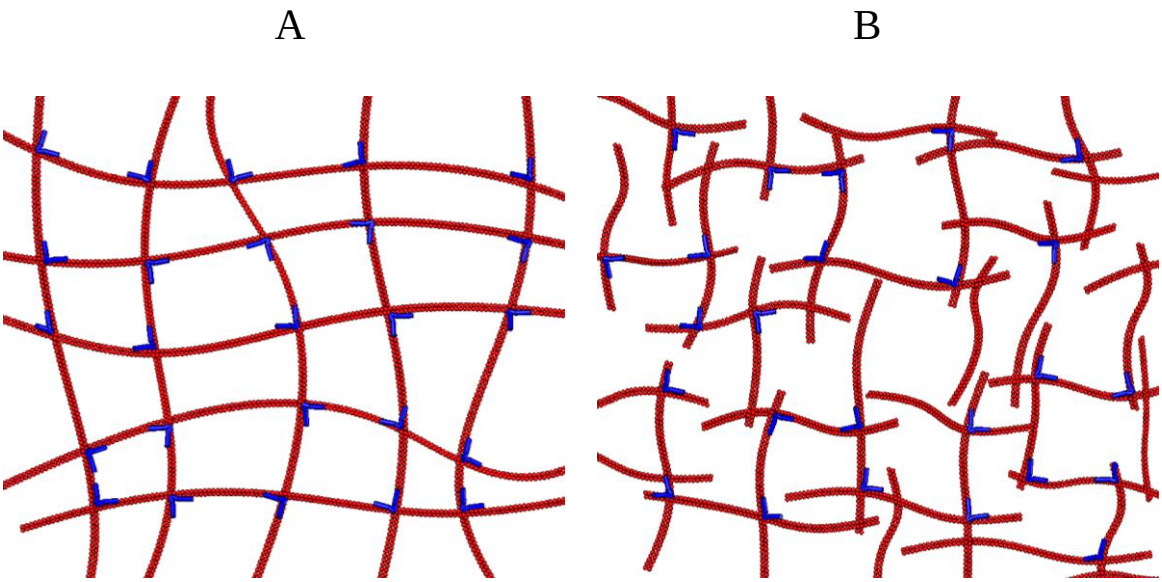

Fig. 10